SERS-Encoded Gold Nanostars for Multiplexed Cell Discrimination

Dorleta Jimenez de Aberasturi,[†#∥] Ana B. Serrano-Montes,[†#] Judith Langer,[†∥]

Malou Henriksen-Lacey[†,∥], Wolfgang J. Parak[†Ł], Luis M. Liz-Marzán*[,†,‡,∥]

[#]*These authors contributed equally*

[†]CIC biomaGUNE, Paseo de Miramón 182, 20009 Donostia-San Sebastián, Spain

[Ł]Fachbereich Physik, Philipps Universität Marburg, Marburg, Germany

[‡]Ikerbasque, Basque Foundation for Science, 48013 Bilbao, Spain

[∥] CIBER de Bioingeniería, Biomateriales y Nanomedicina, CIBER-BBN, 20009 Donostia-San Sebastián, Spain

*e-mail: llizmarzan@cicbiomagune.es

Keywords: SERS-Encoded nanoparticles, Multiplexing, Cell discrimination, SERS imaging.

ABSTRACT

Labeled nanoparticles have attracted much interest toward applications in bioimaging and diagnostics. In particular, surface enhanced Raman scattering (SERS) nanotags have been demonstrated to be excellent candidates for multiplexed imaging and biological detection. We propose an alternative, effective method to easily prepare gold nanostars exhibiting plasmon bands in the near infrared range, encoded with Raman reporter molecules, concomitantly acting as capping agents which are then protected with an amphiphilic polymer. The resulting nanotags are non-cytotoxic and display long-term stability against aggregation and reporter leakage, whilst

showing reproducible SERS signals suitable for multiplexing. These tags were used to distinguish five different types of breast cancer cells by imaging of a *quintuple* cell co-culture. Time-lapse SERS imaging of the co-culture was additionally performed, demonstrating the applicability of these nanotags for cell tracing over time scales above 24 h.

Surface enhanced Raman scattering (SERS) spectroscopy is a versatile method for ultrasensitive detection and quantification of molecules that are located very close or bound to a nanostructured plasmonic metal surface. While unambiguous identification is provided by the characteristic vibrational fingerprint of each molecule, detection limits down to pM and even fM concentrations can be readily obtained.[1–3] In the context of biological analysis, the extremely low intrinsic Raman cross section of most biomolecules often requires the use of other labeling molecules with comparatively higher cross sections as Raman reporters (RaRs). Thus, SERS labeled nanoparticles have recently gained high interest due to their potential for multiplexed bioimaging and sensitive detection of cell types.[4] A SERS label or nanotag comprises a noble metal nanoparticle, which acts as the Raman signal amplifier, covered with a monolayer of RaR molecules acting as fingerprint markers.[5] Advantages of such SERS labels include size and shape tunability, high photostability,[6] low cytotoxicity of gold nanoparticles (AuNPs),[7] and narrow spectral width (~1 nm).[8] When comparing with other systems such as QDs[9–11] with broader spectral width (~30-50 nm) and potential toxicity,[10,12] fluorophores that can show significant spectral overlap[13] (~50 nm),[14] or big silicon microparticles,[15] SERS tags appear particularly attractive for *in vitro* and *in vivo* multiplexing and bioimaging.[16–20]

In bioanalytical applications *in vitro*, cell cultures are commonly used as models to mimic *in vivo* tissues. Models comprising sophisticated co-cultures of different cells are increasingly being studied,[21–23] including 3D cell cultures that imitate tissues such as breast cancer[24] or the

respiratory tract.[25] However, with the increased complexity of such models, methods to specifically identify different cells are needed. New techniques are emerging for screening large amounts of cells, such as CyTOF,[26] but which are destructive to cells. In this context, the use of SERS tags for non-destructive multiplexed cell and tumor imaging has advanced significantly.[4] Wang et al. for example investigated the performance of different SERS NPs under clinically relevant conditions, showing *in vitro*, *ex vivo* and *in vivo* data. [27]The study also confirmed the feasibility of SERS NPs for ratiometric imaging. In previous studies it has also been shown that multiplex SERS labels could be used to differentiate up to three cell lines by targeting surface expressed antigenic markers.[20,28–30] Moreover, breast cancer cells have also been identified with single and multiplexed SERS labels based on different SERS signal intensities.[31–33] However, there are still challenges that have to be resolved to optimize SERS imaging, such as the simple preparation of NPs with long-term stability, showing high, reliable SERS signals over long time scales.[4]

In the design of a SERS nanotag for biological applications, the choice of plasmonic AuNP-RaR combination is of high importance. The excitation with wavelengths ranging from the red to the near infrared (NIR), within the so-called "biological transparency window", should be considered to maximize radiation penetration[34,35] and minimize tissue auto-fluorescence.[36,37] Therefore, much progress has been made toward the preparation of SERS-labeled AuNPs with localized surface plasmon resonances (LSPRs) in this spectral range.[5,38] It has been shown that the LSPRs of branched AuNPs, such as Au nanostars (AuNSs), can be tuned by variation of their aspect ratio,[39] while the high electromagnetic field (EM) enhancements at their sharp tips render AuNSs superior Raman-enhancing substrates as compared to isolated spherical AuNPs.[40,41] Additionally, SERS labels are usually embedded into an external coating to improve stability and protection.[5] This has an important role in preventing: *(i)* leaching of RaR molecules; *(ii)* NP

contamination from interfering molecules in the medium; *(iii)* lowering eventual toxicity of NPs and *(iv)* undesired intensity variations due to plasmon coupling induced by NP-NP interactions.[42] With these requirements in mind, the most commonly employed encapsulation strategies include the use of peptides or proteins,[43–48] liposomes,[49–51] silica[6,52–57] or polymers.[28,58–63] Whilst silica offers some interesting advantages such as biodegradability[64] and ease of use for both *in vitro*[16,54,55] and *in vivo* systems,[18,19,65] it is unfavorable as a coating material for studies in which long-term exposure to cell media is required, due to degradation[66,67] and agglomeration[68] problems. Polymers such as PEG[28,29] or poly(N-isopropylacrylamide)[60] have been also used but the necessary fine-tuning of polymer/RaR ratio, due to the binding competition to the metal surface between stabilizer and reporter, can result in decreased SERS signal intensity. Amphiphilic polymers, such as dodecylamine modified polyisobutylene-alt-maleic anhydride (PMA) have also been extensively employed for the encapsulation of different kinds of NPs showing high stability[63] under biological conditions.[61,62,69] As amphipilic polymers wrap NPs due to hydrophobic interactions, these can be used to coat SERS nanotags without compromising the number of hydrophobic RaR molecules added to their surface. Therefore, coating SERS-encoded AuNPs using PMA is a promising method, which however has not been exploited so far. In this context, we present an alternative method to prepare highly stable SERS tags with excellent SERS performance, based on the transfer of AuNSs to organic solvents using the maximum loading of RaR molecules as stabilizing ligands, and subsequent wrapping with the amphiphilic polymer PMA via hydrophobic interactions. We recently reported that AuNPs of different sizes and shapes can be functionalized with a mixture of dodecanethiol (DDT) and PEG, transferred into organic media and subsequently coated with PMA.[70] Thus, based on this strategy, we combined the use of aromatic hydrophobic thiols as RaRs, which not only bind firmly to the gold surface generating a high Raman signal, but concomitantly act as capping

agents intercalated between PEG pre-stabilized AuNSs and a final PMA protective coating. We first characterized SERS nanotags in solution and then analyzed their ability to image and/or distinguish various single-cell cultures or co-cultures, predominantly for cells of epithelial origin. We specifically focused on breast cancer, the second leading cause of cancer death in women.[71] This is a highly heterogeneous disease in that not only someone with breast cancer can have multiple cancer cell types present, but also in that the cancer cells themselves vary widely.[72] We chose various breast cancer cell lines from subtypes including HER2 positive (SK-BR3), Hormone receptor-positive (MCF-7 and CAMA1) and Triple-negative (HCC1395 and MDA.MB.231). SERS imaging allowed us to distinguish individual cells in a quintuple cell co-culture, thereby highlighting the multiplexing ability provided by these AuNS-based SERS labels. Moreover, time-lapse SERS imaging over 24 hours was also carried out confirming SERS signal stability and reliability in a multi-cell culture.

RESULTS AND DISCUSSION

The preparation of SERS-encoded AuNSs is schematically illustrated in **Figure 1**. AuNSs are first synthesized and stabilized with thiolated PEG; phase transfer from water into $CHCl_3$ is then induced by vigorously stirring the AuNS colloid with a $CHCl_3$ solution of the Raman active molecules, followed by overcoating with the amphiphilic polymer PMA (**Figure S1**).

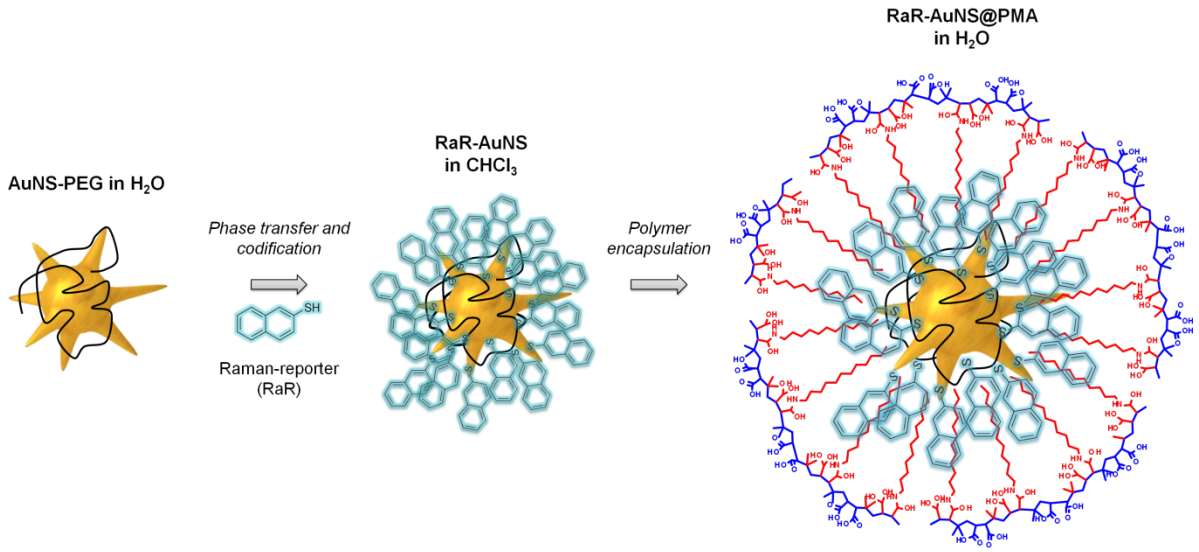

Figure 1. Schematic representation of the preparation of SERS-encoded AuNSs. AuNSs pre-stabilized with PEG are coated with the Raman tag during phase transfer from water into $CHCl_3$. The obtained hydrophobic AuNSs are then wrapped with PMA, leading to encoded AuNSs that are colloidally stable in water. The different elements in the NP construct are not drawn to scale.

Two main conditions are essential to ensure successful phase transfer and codification of AuNSs: *(i)* the Raman-active molecules must be soluble in $CHCl_3$, so that they serve as stabilizing agents during the phase transfer; *(ii)* thiol or amine-terminated Raman molecules should be used, which can strongly bind to the Au surface, thereby facilitating fast phase transfer and avoiding leaching of the SERS tag form the Au surface at a later stage. The encoding strategy presented here favors all these conditions and maximizes the SERS signal by providing close contact of the molecule with the AuNS surface. Benzenethiol (BT), 1-naphthalenethiol (1-NaT), 2-naphthalenethiol (2-NaT), 4-methylbenzenethiol (4-MBT) and biphenyl-4-thiol (4-BPT), are all $CHCl_3$ soluble thiols which bind covalently to the Au surface, have relatively high Raman cross sections and clearly distinguishable fingerprints. 4-Mercaptopyridine (4-MP) presents however a rather low solubility

in $CHCl_3$ and therefore complete phase transfer typically requires longer incubation times, as well as the addition of a base to deprotonate the pyridine ring and decrease its solubility in water. To avoid any undesired nanoparticle aggregation, pre-stabilization of AuNSs with PEG appears to be a critical step, as previously reported.[63,70] The addition of the RaR molecule without previous PEG stabilization leads to irreversible aggregation. Importantly, when AuNSs are protected with a few molecules of PEG/particle, high surface coverage with the RaR can be achieved, thereby ensuring both good SERS performance and colloidal stability (**Figure S2**). Upon transfer into $CHCl_3$, a red shift of the LSPR maximum can be observed for all AuNS codes due to the increase in solvent refractive index. The LSPR bands are however not broadened (**Figures 2A-F**), which indicates high colloidal stability favored by steric repulsion provided by the hydrophobic ligands. Furthermore, in agreement with previous reports,[70,73] reshaping of surfactant-free AuNS is prevented by surface capping with thiolated compounds, *i.e.* codification also provides surface passivation.

Since biological applications require water soluble and highly stable NPs, the particles were encapsulated with PMA after SERS encoding, which results in water solubility thanks to PMA's hydrophilic backbone. The hydrophobic functionalized nanoparticles were wrapped with the polymer *via* hydrophobic interactions between the multiple aliphatic chains of the polymer (dodecylamine chains) and the hydrophobic RaR capping ligands (codes). After coating and dispersion in water, a slight LSPR blueshift was observed, as expected for the lower refractive index of water, as compared to chloroform (**Figures 2A-F**). **Figure 2G-L** shows representative TEM images of PMA-coated SERS tags, invariably displaying well dispersed particles with sharp tips. When negative staining was used, a white shell surrounding the star-shaped NPs can be clearly observed, corresponding to the organic layer wrapping the particles (**Figure 2G-L** insets and **Figure S3**).

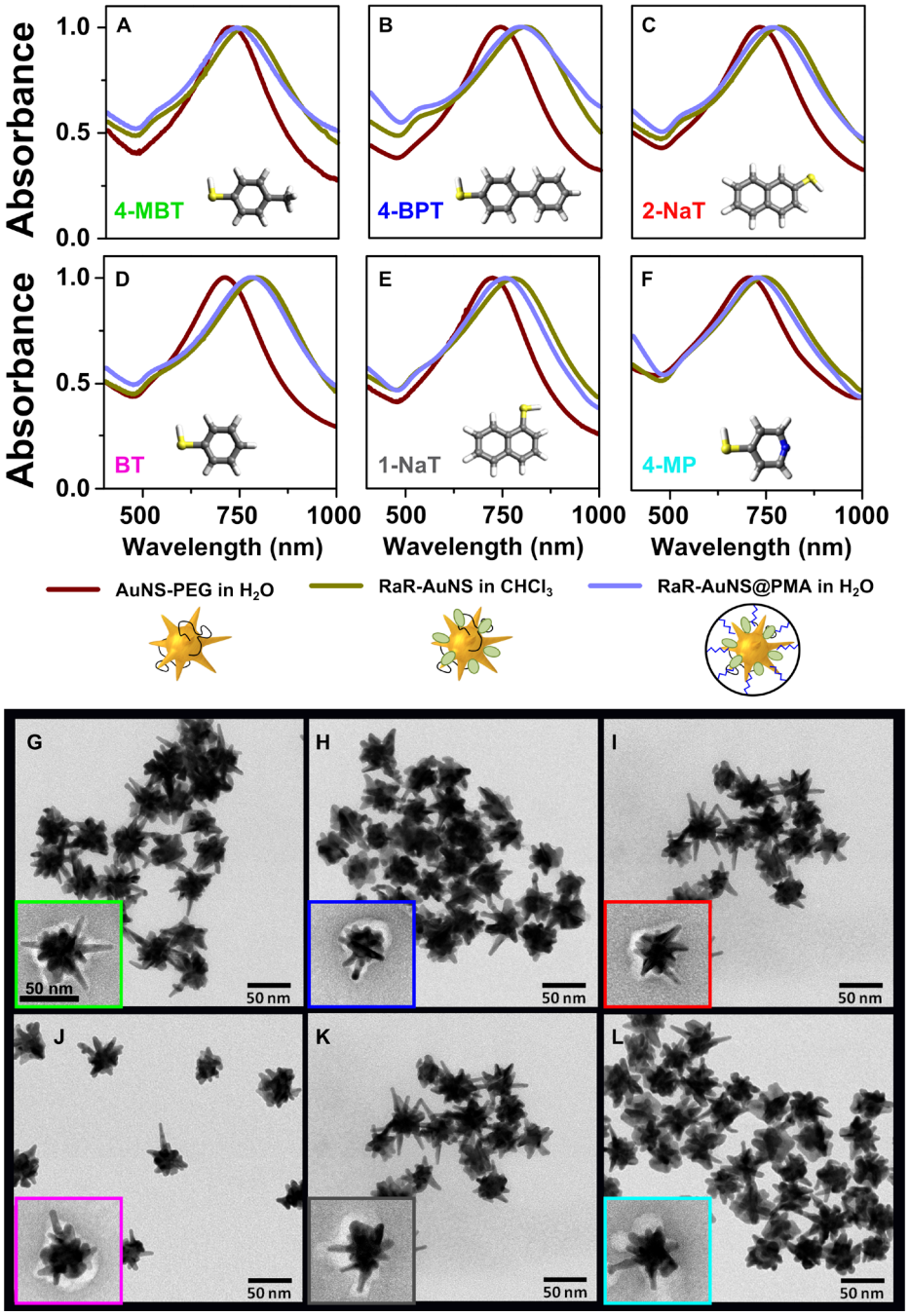

Figure 2. (**A-F**) Normalized Vis-NIR spectra of PEG-AuNSs prior to codification (AuNS; red), after coating with the respective Raman active molecules (RaR-AuNS; green) and after PMA encapsulation (RaR-AuNS@PMA; blue) using different Raman reporters: from left to right, 4-MBT, 4-BPT, 2-NaT, BT, 1-NaT and 4-MP. Molecular structures are displayed as insets. (**G-L**)

TEM images of RaR-AuNS@PMA corresponding to the spectra shown in **A-F**, respectively. Insets: TEM images of negatively stained particles with uranyl acetate.

The long-term stability of the SERS tags was studied by Vis-NIR spectroscopy and TEM. Shown in **Figure 3** are the spectral evolutions of bare AuNSs and AuNS SERS tags. A significant LSPR blueshift was observed for uncoated AuNSs, indicating reshaping into particles with shorter and more rounded tips, which was confirmed by TEM (**Figure 3C**). On the contrary, the plasmon band of PMA-coated AuNSs remains unaltered for long periods of time (months), in agreement with the preserved sharp tips (**Figure 3D**).

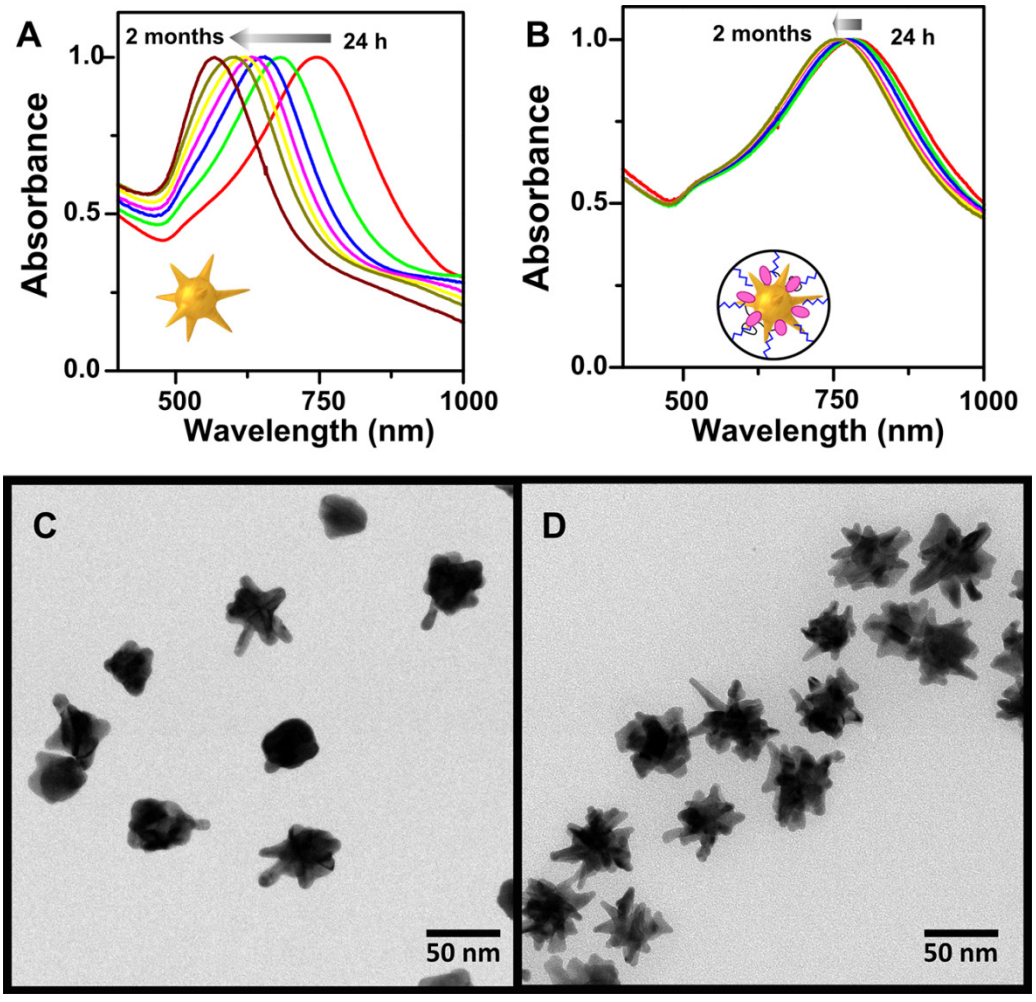

Figure 3. Normalized Vis-NIR spectral evolution (**A**, **B**) and TEM images obtained two months after particle synthesis of bare AuNSs (**C**) and BT-encoded AuNS SERS tags (**D**).

Preserving the spiky structure of SERS encoded particles is important to maintain the LSPR in the NIR, as well as the intrinsic hot spots at the tips,[38,40,41,74] which are essential towards efficient enhancement of the Raman signal using the 785 nm laser in the biological transparency window.[35] Importantly, using the same strategy to synthesize 1-NaT-encoded spherical AuNPs (diameter 100 nm) does not result in a measurable SERS signal when excited at 785 nm due to the lack of coupling between laser light and LSPR (**Figure S4**). This therefore also suggests that the PMA polymer coating efficiently prevents particle aggregation in solution, which has been shown to be responsible for strongly enhanced SERS at 785 nm using nanospheres.[75,76]

Figure 4 shows the SERS spectra of all nanotags, each represented by a different color, as labeled. The corresponding molecular structures (highlighted with the corresponding color) were created and optimized by force field (MMFF94) calculations using the Avogadro Software package.[77] The same color code was used to label all SERS spectra and mappings within this article. SERS measurements of each tag in solution revealed the complete fingerprints of the corresponding encoded RaRs, with no additional signal originating from the polymer. As the total number of vibrations for all the tag molecules are too plentiful to be discussed in the scope of this article, we listed a set of the most dominant vibrations together with the assignment for each RaR in **Table S1** (SI). For the same particle concentration, the highest SERS signal was generated by tags containing 4-BPT, followed by 2-NaT and 4-MBT codes, whereas one order of magnitude lower intensities were recorded from BT and 1-NaT, and 4-MP. These differences may not only be related to different molecular Raman cross sections, but also to variations of RaR density at the AuNS surface due to different binding affinities and to the varying stability in $CHCl_3$.

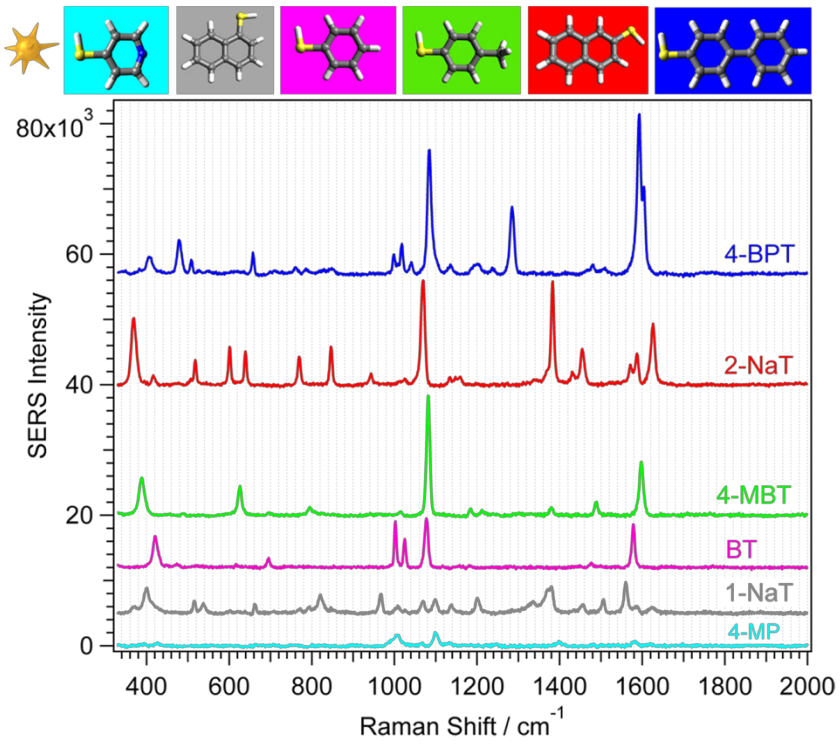

Figure 4. Averaged SERS spectra for six differently encoded SERS tags measured in solution at a concentration of $7.8 \cdot 10^{10}$ NP mL^{-1}, P_{laser} = 18.4 mW for 785 nm and t_{int} = 10 s with 10× objective (NA=0.35). Each color represents a different RaR code, as labeled.

In order to estimate the detection limit of nanotags in solution (under the same experimental conditions) we measured the dependence of SERS intensity on AuNS concentration for the five labels (**Figure S5**). The threshold concentration we could reliably detect was 0.005 mM [Au^0] corresponding to $7.8 \cdot 10^8$ NP mL^{-1}. Roughly estimating the focal volume as a product of laser illumination area (20 µm x 1 µm) and field depth z, the number of AuNS contributing to the SERS signal can be approximated as 40. As the parameter z we used 2.6 mm deduced from the full-width-at-half-maximum (FWHM) of SERS intensity depth profile by recording spectra at different z values. It is noteworthy that SERS studies on cells were performed under different conditions such as the objective (40× immersion, NA=0.8) and support material (quartz glass) and thus affecting the AuNS detection threshold. With the same concentration limit of $7.8 \cdot 10^8$

NP mL^{-1} (experimentally determined for 4-MBT) and a significantly lower z value of 0.42 mm, the minimum number of detectable of AuNS was reduced to approximately 7.

As a first proof of concept, the applicability of the SERS tags to distinguish cells was carried out by incubation of the tags in J774 macrophages, which are known for their phagocytic ability. J774 cells were individually incubated with all six labels, keeping the AuNS concentration and incubation time constant for each system. After several washing steps the SERS spectra in the J774 cultures were analyzed, thereby providing an estimate of the (relative) uptake efficiency of the nanotags, which is important for SERS studies in co-cultures. SERS signals were only recorded at the areas where the J774 cells are present (**Figure 5**). SERS maps in the same figure were created by plotting the intensity of a specific vibration for each RaR, which is typically the most intense one (except for 4-BPT), namely 1083 cm^{-1} (4-MBT), 1284 cm^{-1} (4-BPT), 1381 cm^{-1} (2-NaT), 1000 cm^{-1} (BT), 1558 cm^{-1} (1-NaT) and 1132 cm^{-1} (4-MP). The same molecule-specific vibrations were applied for all subsequent SERS maps, always retaining the same color code. From these images we conclude that *(i)* SERS signal is exclusively detected from J774 cells for all label types and no signal is found from free tags in solution or attached to the glass support; *(ii)* all J774 cells yield measurable signals indicating that SERS is sensitive enough for the present uptake level, and *(iii)* all RaR spectra are not affected by the cell environment indicating good RaR protection by the polymer within the cell culture, except for 4-MP, which displays different fingerprints in solution and with J774. It is noteworthy to mention that the lack of confocal scanning and limited lateral resolution makes SERS nanotags appear to be present throughout the entire intracellular area, yet they are most likely limited to endosomal or lysosomal compartments.[78]

We additionally tested the application of SERS tags to other cell lines and found that RaR signals could be successfully detected in human cells of different tissue origin, such as A549 (bronchial epithelial cell), MDA.MB.435S (melanoma cells) and HUVEC (endothelial cells), combined with BT, 2-NaT and 4-BPT respectively (**Figure S6** in SI).

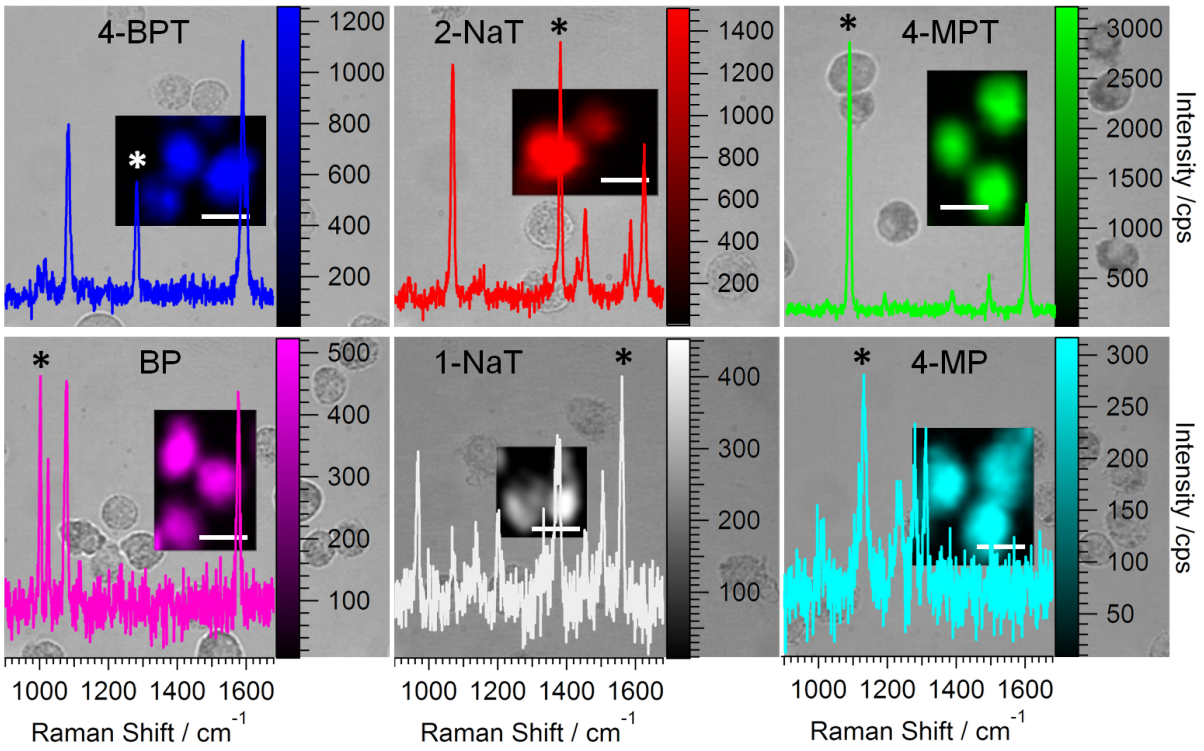

Figure 5. Bright-field optical images overlaid with colored SERS maps, showing several J774 macrophages labeled with six different SERS tags. The corresponding SERS spectra are also plotted on each image. The signals marked with * indicate the specific signals selected for SERS mapping. The white scale bars correspond to 20 μm.

Discrimination of breast cancer cells

An important application for this system is the profiling of various different cell types, such as different breast cancer cells, over extended periods of time using SERS bioimaging. As the

successful detection of cells is strongly dependent on nanotag loading within the cell, we also confirmed the uptake of SERS tags by fluorescence imaging using PMA fluorescently modified with the dye TAMRA (PMA_{TAMRA}) during preparation of the RaR-AuNS (SI, **Section 8**). Then, five different breast cancer cell lines – HCC1395, SK-BR3, MDA.MB.231, CAMA1 and MCF-7 - were incubated overnight with BT-encoded AuNS@PMA_{TAMRA}, at a concentration of $1.6 \cdot 10^{10}$ NP mL^{-1}. NP uptake was confirmed for all cells and intracellular presence (most likely inside compartments such as endosomes or lysosomes) was confirmed by z-stacks using confocal microscopy[11,79] (**Figure S10A**) and TEM micrographs (**Figure S11**). These results suggest a high biocompatibility of the tags, which was further confirmed by cell viability tests (**Figure S12**). We also found that uptake of TAMRA-labeled NPs could be correlated with dark-field microscopy (DFM) images, where the signal arises from light scattering by AuNSs, which confirms the integrity of the SERS tags after cell uptake (**Figure S10B**). As some cells appeared to show higher levels of uptake depending on the nature of the cells, these were subsequently paired with SERS tags expressing weaker Raman signals, and *vice versa*. For SERS studies, breast cancer cells were incubated with the tags under the same conditions. After thorough washing of non-endocytosed particles, cells were transferred onto quartz glass "Small Well" or "Large Well" slides for both individual and *quintuple* SERS analysis, *i.e.* one-cell type and five-cell types co-cultures, respectively. To demonstrate that the designed SERS nanotags can be used to label different kinds of cells, we used two different combinations of cell-RaR, herein termed C1 and C2, for bioimaging and cell identification experiments (see **Table 1**).

Table 1. Sets for the RaR label-breast cancer cell combinations C1 and C2 and detection probability for set C2, calculated from single-point SERS maps of the single-cultures shown in **Figures S13-15**. Minimum number of analyzed cells was 100.

Combination	Cell type				
	SK-BR3	HCC1395	MCF-7	CAMA1	MDA.MB.231
C1	1-NaT	BT	4-BPT	4-MBT	2-NaT
C2	4-BPT	4-MBT	2-NaT	BT	1-NaT
Detection probability (%)	83±12	90±11	87±7	72±9	73±19

Shown in **Figure 6** are 2D SERS maps corresponding to C1, which confirms that the specific SERS signals were detected for all five cell lines, but that the intensity can vary strongly for each cell type and for each RaR label. In few cases unbalanced nanotag uptake can lead to some cells being (nearly) undetectable by SERS (*e.g.* SK-BR3 with the low-intensity 1-NaT in **Figure 6A** and CAMA1 with the high-intensity 4-MBT in **Figure 6B**). To evaluate the detection probability of specific cell lines, statistical SERS measurements (one spectrum per cell = single-point maps) of at least 100 individual cells per type were performed. As an example, the single–point SERS map in **Figure 6F** indicates that 4-BPT was detected in 98 % of all measured MCF-7 cells. SERS imaging of the single-cell cultures in C2 was found to yield results that are qualitatively similar to those in C1 (**Figures S13-S15** in SI). Corresponding C2 cell detection probabilities were calculated from single-point SERS mappings (**Figures S13-S15** in SI) and summarized in **Table 1**.

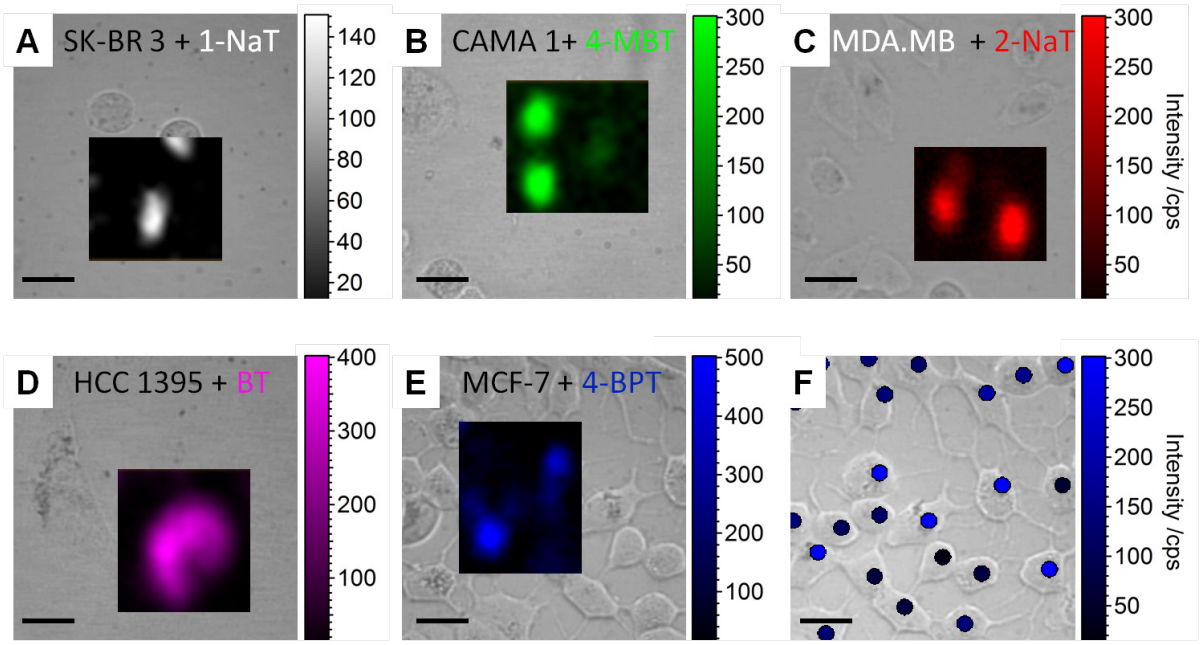

Figure 6. (**A-E**) Correlated transmitted light and SERS images of breast cancer cells corresponding to the cell-RaR combination C1. (**F**) Statistical SERS measurements by single-point SERS mapping of cells marked with 4-BPT tags allow fast analysis for high cell detection efficiency (here: 4-BPT is found in 98% of measured MCF-7 cells). The black scale bars correspond to 20 µm.

We finally imaged a *quintuple* breast cancer cell co-culture composed of cells which were pre-incubated with their corresponding SERS nanotags as defined in combination C2. For cell discrimination the entire fingerprint was compared to reference spectra obtained from the single-cell samples (**Figure 7A**), assigned to the relevant RaR. The resulting SERS image (**Figure 7B**) shows the relative distribution of cell lines in the scanned area. The five RaRs can be clearly differentiated, corresponding to the presence of the five different breast cancer cells within the co-culture. To evaluate the reliability of this cell discrimination method and quantify larger areas in cell mixtures, different positions of the sample were analyzed by single-point SERS mapping. The result of the composition map for the largest area (= 0.22 mm^2) containing 147 cells is

shown in **Figure 7C** and the detailed quantitative analysis of cell population is summarized in **Figure 7D**. In this particular case, 84% of the total amount of cells measured were unambiguously distinguished, whereas 16% (black dots in **Figure 7C**) could not be identified, probably due to the NP load being too low.

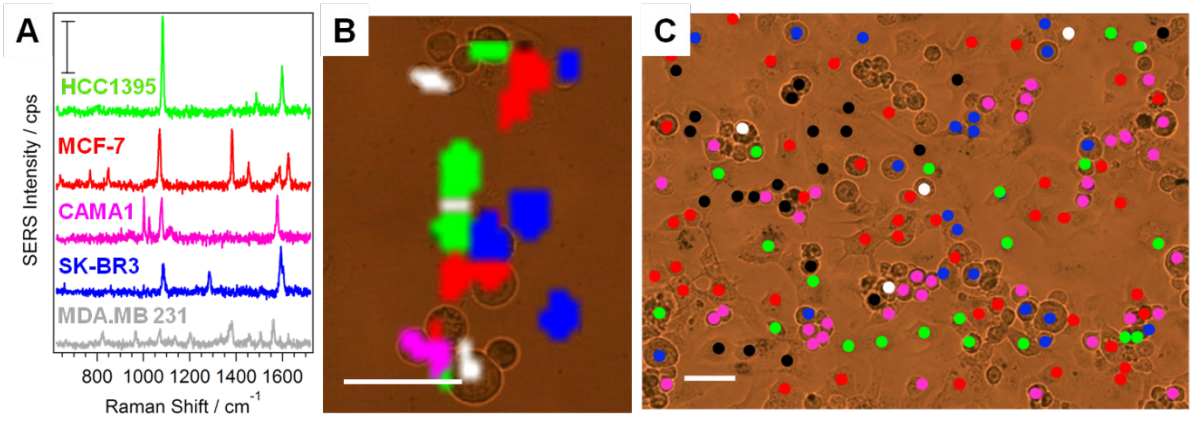

D

Assigned Cell type	SK-BR 3	CAMA 1	HCC 1395	MDA.MB 231	MCF-7	no signal
Population in (c)	15%	24%	13%	3%	29%	16%

Figure 7. Compositional assignment of a *quintuple* cell mixture using RaR labeled SERS nanotags according to set C2. (**A)** Reference RaR fingerprints recorded from the single-cultures; (**B)** bioimaging with cell assignment; and (**C**) large-scale SERS single-point mapping to quantify the composition of 147 cells within an area of 0.22 mm^2 using references from **A**. Black dots correspond to cells with too low signal. (**D)** Summarized quantitative cell population in **C**. The vertical (black) intensity scale bar in **A** corresponds to 500 cps, and the horizontal (white) scale bars in **B** and **C** correspond to 50 µm.

Time-lapse SERS imaging

Bioimaging of living cells is often confronted with the problem that the culture evolves due to cell motion, growth, cloning and death. Cell dynamics and chemical changes are also known to

affect the long-term fate of internalized NPs. Therefore, SERS tags might be degraded, excreted or transferred to daughter cells leading to "dilution" of the signal. Therefore, proof for successful bioimaging, reliable discrimination and tracing of living cells must also include SERS imaging over periods of time that are longer than those required for cell division to occur. **Figure 8** shows selected time-dependent SERS images for a fixed area within a *quintuple*-cell culture, recorded with time lags of 3-4 h for a total of 29 h. In general, the time-dependent images show a similar color pattern (within the scanned area in the order of 0.1 mm^2), meaning that both the cell culture and the PMA-coated AuNS SERS tags maintain a sufficient stability. We also obtained bright-field images at time 0 and after finishing the time-lapse series, to confirm that the cell distribution does not change significantly (**Figure S16** in SI). Closer inspection of the time-dependent images reveals some changes in relative position and size indicating continuous dynamics within the cell co-culture. Lateral as well as horizontal changes are also supported by the bright-field snapshots in **Figure S16**. Unfortunately, the rough lateral resolution due to a compromise between large image size and minimum integration time does not allow precise tracking of individual cells. Nonetheless, this experiment demonstrates the possibility to trace single cell displacements over long time scales. Depending on the time scale, within the range of minutes to hours, total map size, lateral resolution/scan step distance, integration time and time resolution must be optimized. During time-lapse repetition in a second *quintuple* cell culture significant movements and cell degradation could be detected by SERS in the late stage co-culture (> 24 hours, **Figure S17** in SI). A third SERS imaging experiment indicates precipitation of a few cells also proven by bright-field images before and after the SERS time-lapse (Figure **S18-1** and **S18-2** in SI).

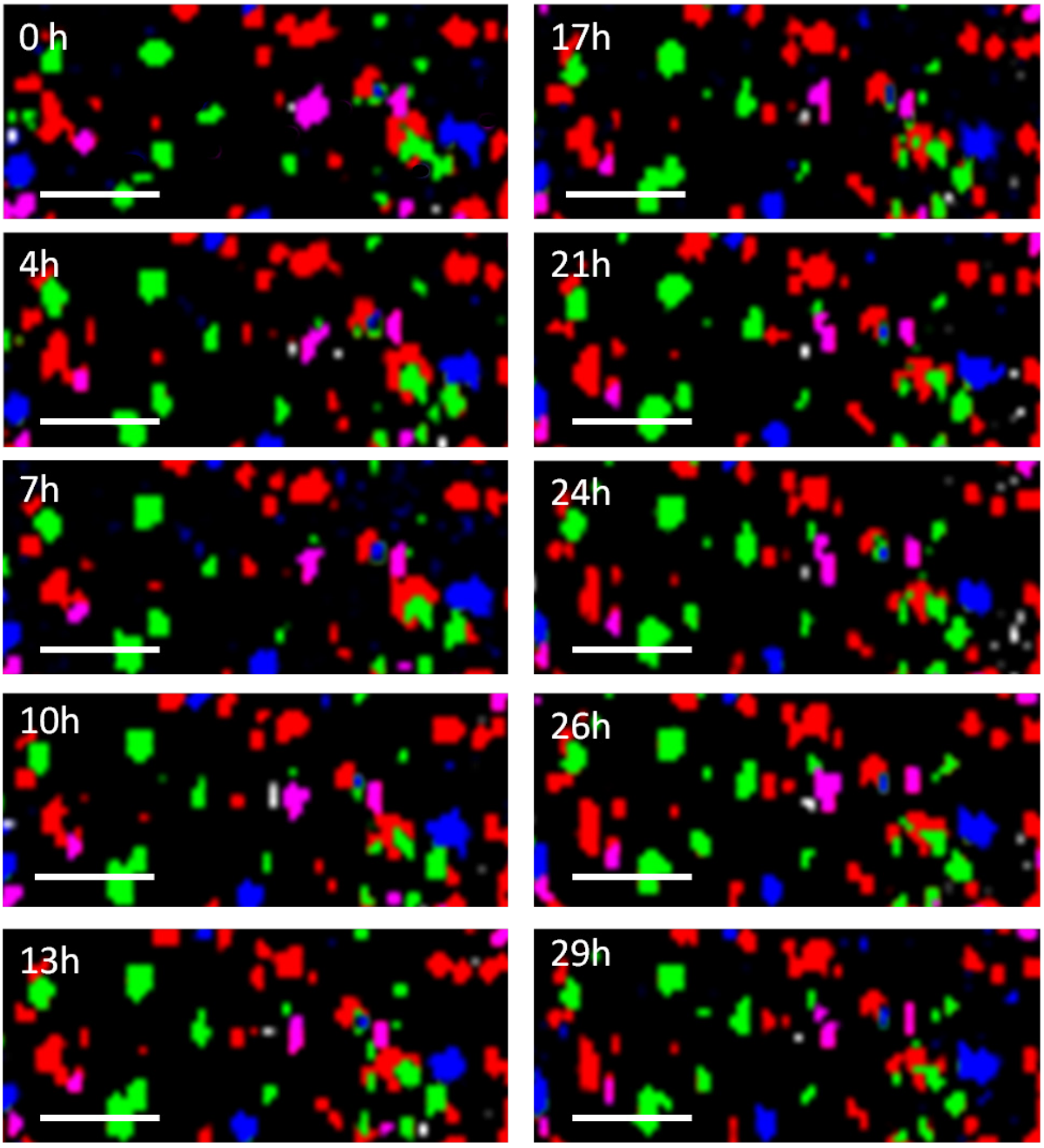

Figure 8. Time-lapse SERS images for a constant area of 0.08 mm^2 from the *quintuple* cell culture over a time span of 29 h. The white scale bar corresponds to 100 μm. Lateral scanning step size was 5.5 μm.

CONCLUSIONS

In summary, we devised and fabricated highly stable, biocompatible, multiplexing SERS nanotags based on PMA-coated gold nanostars with LSPR modes within the first biological transparency window. AuNSs were functionalized with small aromatic and hydrophobic thiols, which act not only as Raman reporters but also as capping agents to drive nanoparticle phase transfer from aqueous to organic media, where subsequent polymer coating is performed. Importantly, the associated SERS signals remain stable even under biological conditions. By taking advantage of cellular endocytosis, these SERS tags can be used to label a wide variety of cell types derived from a range of different tissues. Finally, in a proof-of-concept experiment we successfully demonstrated that single breast cancer cells derived from five different cell lines can be detected, distinguished and imaged within a *quintuple* co-culture by using these nanotags for SERS. We show that SERS signals and images of the cell culture are stable over time periods up to at least 24 h without significant loss of cells from the area being analyzed. The method additionally offers the possibility to accurately identify and trace cells over time by SERS microscopy. Future experiments can be envisaged, to functionalize the polymeric coating of the SERS labels with targeting moieties to specifically bind different cancer cells in co-culture, and to identify single cells from a mixture of different cells by a multiplex assay. The rapid identification of different breast cancer cells from a mixed culture offers hope for improved and faster diagnosis, and the optimization of treatment therapies in the future. The method can be further extended to multiplexed phenotyping of different cells or cell labeling in 3D cellular models, thus offering new opportunities toward biomedical applications.

METHODS

Materials. Milli-Q water (resistivity 18.2 MΩ·cm) was used in all experiments. Hydrogen tetrachloroaurate trihydrate ($HAuCl_4 \cdot 3H_2O$, ≥99.9%), sodium citrate tribasic dihydrate (≥98%), silver nitrate ($AgNO_3$, ≥99%), L-ascorbic acid (AA, ≥99%), O-[2-(3-mercaptopropionylamino) ethyl]-O'–methylpolyethylene glycol (PEG, MW 5,000 g/mol), benzenethiol (BT, ≥98%), 1-naphthalenethiol (1-NaT, 99%), 2-naphthalenethiol (2-NaT, 99%), 4-methylbenzenethiol (4-MBT, 98%), biphenyl-4-thiol (4-BPT, 97%), 4-mercaptopyridine (4-MP, 95%), poly(isobutylene-alt-maleic anhydride), (average Mw ~6,000 g/mol), dodecylamine (98%) and chloroform ($CHCl_3$, ≥99.8%) were purchased from Sigma-Aldrich. Tetramethylrhodamine cadaverine (TAMRA, λ_{ex} = 544 nm, λ_{em} = 571 nm, #A1318) was purchased from Life Technologies (Invitrogen). Hydrochloric acid solution (37 wt%) was purchased from Panreac. All glassware was washed with aqua regia, rinsed 3-fold with Milli-Q water and dried before use.

Synthesis of Gold Nanostars. AuNSs were prepared by seed-mediated growth.[80] The seed solution was prepared by adding 5 mL of 34 mM citrate solution to 95 mL of boiling 0.5 mM $HAuCl_4$ solution under vigorous stirring. After 15 min of boiling, the solution was cooled down and stored at 4 °C. For the synthesis of 50 nm AuNSs with LSPR maximum at 750 nm, 2.5 mL of the citrate-stabilized seed solution was added to 50 mL of 0.25 mM $HAuCl_4$ solution (with 50 µL of 1 M HCl) in a 20 mL glass vial at room temperature under moderate stirring. Quickly, 500 µL of 3 mM $AgNO_3$ and 250 µL of 100 mM ascorbic acid were added simultaneously. The solution rapidly turns from light red to greenish, indicating AuNSs formation. The resulting solution was mixed with 410 µL of PEG-SH 0.1 mM and stirred for 15 min, washed by centrifugation at 1190 g, 25 min, 10 ºC and redispersed in water.

Polymer preparation. The amphiphilic polymer, PMA, was prepared as previously reported.[81,82] During preparation, 75 % of the anhydride rings from the polyisobutylene-alt-maleic anhydride hydrophilic backbone were reacted with dodecylamine ligand, leaving 25 % free. For fluorescence imaging of cells with AuNSs, 2 % of these anhydride rings were modified with TAMRA (see SI **Section 8**).

Gold nanostar codification. AuNSs were coated with the corresponding Raman reporter molecule (4-MP, 1-NaT, BT, 4-MBT, 2-NaT, 4-BPT) *via* organic phase transfer, by adapting previous work.[70] Specifically, instead of using DDT, Raman-active molecules were incorporated as capping ligands. PEG pre-stabilized AuNSs (2.5 mL, [NP] ~ $2.34 \cdot 10^{11}$ NP mL^{-1} corresponding to [Au^0] = 1.5 mM, as determined from the absorbance at 400 nm[83] and assuming the AuNS surface is that of a 50 nm diameter sphere) was gently stirred with a $CHCl_3$ solution of the Raman reporter. The number of added RaR molecules was calculated to be 155 molecules per nm^2. Phase transfer occurred after vigorous stirring for periods between 15 min and 1 hour. The transfer with 4-MP was assisted by addition of 250 μL NaOH 1 M and required stirring overnight. Upon transfer to $CHCl_3$, the organosols were purified by centrifugation (1320 g; 25 min; 10 ºC) to remove excess of free thiols. Precipitation was facilitated by adding ethanol to the chloroform solution (1:5). Samples were stored at 4 ºC until further use.

Polymer encapsulation. For secondary coating of the SERS encoded NPs with PMA, the AuNS solutions (2.5 mL, [NP] ~ $1.56 \cdot 10^{11}$ NP mL^{-1}) in $CHCl_3$ were mixed with a solution of PMA in $CHCl_3$ ($V_{Polymer}$ = 15.5 μL, $c_{Polymer}$ = 0.05 M, $R_{p/area}$ = 150 nm^{-2}) in a 25 mL round bottom beaker. The mixture was stirred and the solvent was slowly evaporated. The resulting solid films containing NPs were dissolved in 28 mM sodium borate buffer at pH = 12.[70] After polymer coating the particles were purified and the concentration adjusted to ~ $7.8 \cdot 10^{10}$ NP mL^{-1} (more details in SI **Section 1**).

Cell culture. SK-BR3 and HCC1395 were purchased from ATCC (LGC Standards, Barcelona). CAMA1, J774, MDA.MB.231, MCF-7, MDA.MB.435s, HUVEC and A549 cells were kind gifts from collaborators at CIC biomaGUNE. All cells with the exception of SK-BR3 and HUVEC were grown in DMEM media supplemented with 10% fetal bovine serum (FBS) and 1% penicillin-streptomycin (PS). HCC1395, CAMA1 and MCF-7 media was supplemented with 1% sodium pyruvate. SK-BR3 cells were grown in McCoys media supplemented with 10% FBS and 1% PS, and HUVEC cells were grown in F12-K media supplemented with endothelial cell growth factor (ECGF, 30 μg/mL), heparin (0.1 mg/mL), 10% FBS and 1% PS. All cells were passaged using Trypsin-EDTA with the exception of J774 cells which were passaged by pipetting. Cells were grown in a humidified atmosphere at 37 °C with 5% CO_2. All media and supplements were purchased from Invitrogen.

Cell preparation for microscopy. Cell uptake of PMA_{TAMRA}-coated NPs was imaged using fluorescence and DFM. In some cases cell nuclei and cell membranes were counterstained with 4',6-diamidino-2-phenylindole (DAPI) and wheat germ agglutinin Alexa Fluor 647 (WGA-AF647), respectively (both from Invitrogen). For dark-field imaging cells were grown in glass-bottomed dishes with an etched grid (Ibidi, Germany) so that identical cells could be identified using both fluorescence and DFM (**Figure S10B**) Cells were detached from growth flasks, counted and plated in 96-well cell culture plates at $1 \cdot 10^5$ cells/mL, 100 μL/well. HUVEC cells were plated at approximately a 10-fold lower concentration. In the case of J774 cells, they were plated directly at the same concentration in a specially made cell slide comprising a 1.5 mL Eppendorf tube, with lid removed and a ring cut (few mm) glued onto a quartz microscope 75×25 mm slide (Electron Microcopy Sciences), known herein as "Small Well". Dentist glue (Twinsil, Germany) was used, which is non-toxic and can be easily removed. The total volume was approximately 200 μL. Cells were allowed to adhere for a few hours-overnight before

incubation of SERS tags ([NP] ~ $1.6 \cdot 10^{10}$ NP mL^{-1}) for 18-36 h, followed by extensive washing with PBS to remove non-endocytosed particles. HCC1395, SK-BR3, MDA.MB.231 and CAMA1 cells were removed from the 96-well plate using trypsin-EDTA and split into two batches. One batch, equivalent to 1 well of a 96-well plate (initial cell number 10000 cells), was plated in a Small Well whilst the rest of cells were mixed together, centrifuged (2090 g; 5 min) and resuspended in a total volume of 200 μL complete DMEM media. The cells were added to a larger Small Well (*ca.* 2 cm diameter) to obtain a quintuple culture, each cell line containing a different SERS tag. Wells were covered with Parafilm to prevent evaporation. A549, J774, MDA.MB.435S and HUVEC cells were analyzed as single cultures using the same methods. For single-culture SERS measurements, the cell medium was replaced with PBS. For 36 h time-lapse co-culture SERS measurements, complete DMEM medium was replaced by CO_2 buffering Leibovitz´s L-15 cell medium so as to improve cell viability outside the incubator.

SERS measurements were performed with a confocal Raman microscope (Renishaw inVia) equipped with 1024×512 CCD detectors using a 785 nm laser excitation source (maximum output 270 mW) and a 1200 l/mm diffraction grating. For control and performance, SERS test spectra were collected from 1 mL glass vials (ThermoFisher) containing 500 μL of encoded AuNSs in aqueous solution ([NP] ~ $7.8 \cdot 10^{10}$ NP mL^{-1}), using a 10× objective (numerical aperture NA=0.35) in expanded scan mode with an integration time of 10 s at a laser power of 62 mW and accumulating five scans. SERS measurements in cells were carried out in static mode (center of scattered wavenumber 1200 cm^{-1}) using a 40× water immersion objective (NA=0.8) with 1 s integration time at 15 mW laser power. Single-point SERS maps were recorded by measuring only one spectrum per cell (randomly chosen within the cell area) whereas spectra for SERS imaging were measured on a selected grid with a point to point distances between 2 (**Figures 5,6**) and 5.5 μm (**Figure 8**) in x- and y directions, depending on the total map size. In single-cell

cultures, images and single-point maps were then created by plotting the baseline-corrected intensity of one tag-specific SERS signal (indicated in **Figure 5**), as a function of the position. In *quintuple* cell co-cultures, the spectra were analyzed using the DCLS tool provided by Renishaw software Wire 3.4. Therein, each measured spectrum was compared to the set of five label reference spectra (recorded from single-cultures). Images and single-point maps were created by plotting the label score as a function of the position using a pre-defined color code (here: BT-magneta, 4-BPT-blue, 4-MT-green, white-1-NaT, red-2-NaT). The average laser powers were experimentally determined by means of a thermal laser sensor and a power meter (both from Ophir) in air.

Characterization TEM images were collected with a JEOL JEM-1400PLUS transmission electron microscope operating at 120 kV, using carbon coated 400 square mesh copper grids. UV-Vis optical extinction spectra were recorded using an Agilent 8453 UV-Vis diode-array spectrophotometer. The fluorescence of the NPs was measured with a Horiba Jobin Yvon Fluorolog fluorimeter upon excitation at λ_{ex} = 530 nm. Imaging was performed with a confocal laser scanning microscope (LSM510, Zeiss), equipped with lasers allowing excitation at 405 nm (DAPI), 561 nm (TAMRA) and 633 nm (WGA-AF647), and an Axio Cell observer (Zeiss) with LED excitation at 365 nm and 570 nm for DAPI and TAMRA respectively. For DFM imaging a Nikon Eclipse Ti-U microscope with dark-field oil condenser and a 60× S Plan Fluor objective (NA=0.7) was used. A neutral density (ND) and neutral color balance (NCB) filter was inserted. Photos were taken using 0.1 s exposure with identical light intensity levels and other variables for all samples.

ASSOCIATED CONTENT

Supporting Information

The Supporting Information is available free of charge on the ACS Publications website at DOI: 10.1021/acs.chemmater.xxxx.

Additional details on polymer coating optimization and characterization, including overview TEM images of coated Au NSs; stability analysis of Au NSs, vibrational assignment of SERS labels; analysis of detection limits; additional images of cell SERS imaging and fluorescent labeling; TEM images of encoded Au NSs in cells; cell viability studies.

AUTHOR CONTRIBUTIONS

D.J.d.A. devised and executed the synthesis of encoded nanostars, A.B.S.M prepared and characterized encoded nanoparticles. J.L devised and performed SERS measurements. M.H.L prepared cell cultures and performed *in vitro* experiments. W.J.P. participated in the general concept and guided execution of cell co-culture and tracing experiments. L.M.L.M coordinated the project and guided various experiments. All authors discussed the results, contributed to data analysis, and participated in the preparation of the manuscript.

ACKNOWLEDGMENTS

Prof. Juan Mareque, Dr. Marco Marradi, Prof. Soledad Penades and Dr. Sergio Moya (CIC biomagune) are thanked for providing various cell lines. Funding is acknowledged from the European Commission (Grant #310445-2 SAVVY) and the European Research Council (ERC Advanced Grant #267867 Plasmaquo). WJP and LMLM acknowledge funding from MINECO (project MAT2013-48169-R and MAT2013-46101-R).

REFERENCES

(1) Gao, F.; Lei, J.; Ju, H. Label-Free Surface-Enhanced Raman Spectroscopy for Sensitive DNA Detection by DNA-Mediated Silver Nanoparticle Growth. *Anal. Chem.* **2013**, *85*, 11788–11793.

(2) Li, J.-M.; Ma, W.-F.; You, L.-J.; Guo, J.; Hu, J.; Wang, C.-C. Highly Sensitive Detection of Target ssDNA Based on SERS Liquid Chip Using Suspended Magnetic Nanospheres as Capturing Substrates. *Langmuir* **2013**, *29*, 6147–6155.
(3) Zengin, A.; Tamer, U.; Caykara, T. Fabrication of a SERS Based Aptasensor for Detection of Ricin B Toxin. *J. Mater. Chem. B* **2014**, *3*, 306–315.
(4) Wang, Y.; Kang, S.; Doerksen, J. D.; Glaser, A. K.; Liu, J. T. C. Surgical Guidance via Multiplexed Molecular Imaging of Fresh Tissues Labeled With SERS-Coded Nanoparticles. *IEEE J. Sel. Top. Quantum Electron.* **2016**, *22*, 1–11.
(5) Wang, Y.; Schlücker, S. Rational Design and Synthesis of SERS Labels. *Analyst* **2013**, *138*, 2224–2238.
(6) Doering, W. E.; Nie, S. Spectroscopic Tags Using Dye-Embedded Nanoparticles and Surface-Enhanced Raman Scattering. *Anal. Chem.* **2003**, *75*, 6171–6176.
(7) Dreaden, E. C.; Alkilany, A. M.; Huang, X.; Murphy, C. J.; El-Sayed, M. A. The Golden Age: Gold Nanoparticles for Biomedicine. *Chem. Soc. Rev.* **2012**, *41*, 2740–2779.
(8) McCreery, R. L. In *Raman Spectroscopy for Chemical Analysis;* Winefordner J. D., Eds.; John Wiley & Sons, Inc.: Hoboken, NJ, USA, **2000**.
(9) Rivera-Gil, P.; Yang, F.; Thomas, H.; Li, L.; Terfort, A.; Parak, W. J. Development of an Assay Based on Cell Counting with Quantum Dot Labels for Comparing Cell Adhesion within Cocultures. *Nano Today* **2011**, *6*, 20–27.
(10) Dubertret, B.; Skourides, P.; Norris, D. J.; Noireaux, V.; Brivanlou, A. H.; Libchaber, A. In Vivo Imaging of Quantum Dots Encapsulated in Phospholipid Micelles. *Science* **2002**, *298*, 1759–1762.
(11) Rees, P.; Wills, J. W.; Brown, M. R.; Tonkin, J.; Holton, M. D.; Hondow, N.; Brown, A. P.; Brydson, R.; Millar, V.; Carpenter, A. E.; *et al.* Nanoparticle Vesicle Encoding for Imaging and Tracking Cell Populations. *Nat. Methods* **2014**, *11*, 1177–1181.
(12) Tsoi, K. M.; Dai, Q.; Alman, B. A.; Chan, W. C. W. Are Quantum Dots Toxic? Exploring the Discrepancy Between Cell Culture and Animal Studies. *Acc. Chem. Res.* **2013**, *46*, 662–671.
(13) Abbasi, A. Z.; Amin, F.; Niebling, T.; Friede, S.; Ochs, M.; Carregal-Romero, S.; Montenegro, J.-M.; Rivera Gil, P.; Heimbrodt, W.; Parak, W. J. How Colloidal Nanoparticles Could Facilitate Multiplexed Measurements of Different Analytes with Analyte-Sensitive Organic Fluorophores. *ACS Nano* **2011**, *5*, 21–25.
(14) Lakowicz, J. R. In *Principles of Fluorescence Spectroscopy*; Springer US: Boston, MA, **2006**.
(15) Fernandez-Rosas, E.; Gómez, R.; Ibañez, E.; Barrios, L.; Duch, M.; Esteve, J.; Nogués, C.; Plaza, J. A. Intracellular Polysilicon Barcodes for Cell Tracking. *Small* **2009**, *5*, 2433–2439.
(16) Wang, H.-N.; Vo-Dinh, T. Multiplex Detection of Breast Cancer Biomarkers Using Plasmonic Molecular Sentinel Nanoprobes. *Nanotechnology* **2009**, *20*, 65101.
(17) Matschulat, A.; Drescher, D.; Kneipp, J. Surface-Enhanced Raman Scattering Hybrid Nanoprobe Multiplexing and Imaging in Biological Systems. *ACS Nano* **2010**, *4*, 3259–3269.
(18) Keren, S.; Zavaleta, C.; Cheng, Z.; de la Zerda, A.; Gheysens, O.; Gambhir, S. S. Noninvasive Molecular Imaging of Small Living Subjects Using Raman Spectroscopy. *Proc. Natl. Acad. Sci.* **2008**, *105*, 5844–5849.
(19) Zavaleta, C. L.; Smith, B. R.; Walton, I.; Doering, W.; Davis, G.; Shojaei, B.; Natan, M. J.; Gambhir, S. S. Multiplexed Imaging of Surface Enhanced Raman Scattering Nanotags

in Living Mice Using Noninvasive Raman Spectroscopy. *Proc. Natl. Acad. Sci.* **2009**, *106*, 13511–13516.
(20) Samanta, A.; Das, R. K.; Park, S. J.; Maiti, K. K.; Chang, Y. T. Multiplexing SERS Nanotags for the Imaging of Differentiated Mouse Embryonic Stem Cells (mESC) and Detection of Teratoma in Vivo. *Am. J. Nucl. Med. Mol. Imaging* **2014**, *4*, 114–124.
(21) Miki, Y.; Ono, K.; Hata, S.; Suzuki, T.; Kumamoto, H.; Sasano, H. The Advantages of Co-Culture over Mono Cell Culture in Simulating in Vivo Environment. *J. Steroid Biochem. Mol. Biol.* **2012**, *131*, 68–75.
(22) Rothen-Rutishauser, B.; Blank, F.; Mühlfeld, C.; Gehr, P. In Vitro Models of the Human Epithelial Airway Barrier to Study the Toxic Potential of Particulate Matter. *Expert Opin. Drug Metab. Toxicol.* **2008**, *4*, 1075–1089.
(23) Roggen, E. L.; Soni, N. K.; Verheyen, G. R. Respiratory Immunotoxicity: An in Vitro Assessment. *Toxicol. Vitro Int. J. Publ. Assoc. BIBRA* **2006**, *20*, 1249–1264.
(24) Kim, J. B.; Stein, R.; O'Hare, M. J. Three-Dimensional in Vitro Tissue Culture Models of Breast Cancer — a Review. *Breast Cancer Res. Treat.* **2004**, *85*, 281–291.
(25) Rothen-Rutishauser, B. M.; Kiama, S. G.; Gehr, P. A Three-Dimensional Cellular Model of the Human Respiratory Tract to Study the Interaction with Particles. *Am. J. Respir. Cell Mol. Biol.* **2005**, *32*, 281–289.
(26) Cheung, R. K.; Utz, P. J. SCREENING: CyTOF—the next Generation of Cell Detection. *Nat. Rev. Rheumatol.* **2011**, *7*, 502–503.
(27) Wang, Y. "Winston"; Khan, A.; Som, M.; Wang, D.; Chen, Y.; Leigh, S. Y.; Meza, D.; McVeigh, P. Z.; Wilson, B. C.; Liu, J. T. C. Rapid Ratiometric Biomarker Detection with Topically Applied SERS Nanoparticles. *Technology* **2014**, *2*, 118–132.
(28) Qian, X.; Peng, X.-H.; Ansari, D. O.; Yin-Goen, Q.; Chen, G. Z.; Shin, D. M.; Yang, L.; Young, A. N.; Wang, M. D.; Nie, S. In Vivo Tumor Targeting and Spectroscopic Detection with Surface-Enhanced Raman Nanoparticle Tags. *Nat. Biotechnol.* **2008**, *26*, 83–90.
(29) Dinish, U. S.; Balasundaram, G.; Chang, Y.-T.; Olivo, M. Actively Targeted in Vivo Multiplex Detection of Intrinsic Cancer Biomarkers Using Biocompatible SERS Nanotags. *Sci. Rep.* **2014**, *4*, 4075.
(30) Wang, M.; Cao, X.; Lu, W.; Tao, L.; Zhao, H.; Wang, Y.; Guo, M.; Dong, J.; Qian, W. Surface-Enhanced Raman Spectroscopic Detection and Differentiation of Lung Cancer Cell Lines (A549, H1229) and Normal Cell Line (AT II) Based on Gold Nanostar Substrates. *RSC Adv.* **2014**, *4*, 64225–64234.
(31) Yang, J.; Wang, Z.; Zong, S.; Song, C.; Zhang, R.; Cui, Y. Distinguishing Breast Cancer Cells Using Surface-Enhanced Raman Scattering. *Anal. Bioanal. Chem.* **2011**, *402*, 1093–1100.
(32) Lee, S.; Chon, H.; Lee, J.; Ko, J.; Chung, B. H.; Lim, D. W.; Choo, J. Rapid and Sensitive Phenotypic Marker Detection on Breast Cancer Cells Using Surface-Enhanced Raman Scattering (SERS) Imaging. *Biosens. Bioelectron.* **2014**, *51*, 238–243.
(33) Nima, Z. A.; Mahmood, M.; Xu, Y.; Mustafa, T.; Watanabe, F.; Nedosekin, D. A.; Juratli, M. A.; Fahmi, T.; Galanzha, E. I.; Nolan, J. P.; *et al.* Circulating Tumor Cell Identification by Functionalized Silver-Gold Nanorods with Multicolor, Super-Enhanced SERS and Photothermal Resonances. *Sci. Rep.* **2014**, *4,* 4752.
(34) Weissleder, R. A Clearer Vision for in Vivo Imaging. *Nat. Biotechnol.* **2001**, *19*, 316–317.
(35) Smith, A. M.; Mancini, M. C.; Nie, S. Bioimaging: Second Window for in Vivo Imaging. *Nat. Nanotechnol.* **2009**, *4*, 710–711.

(36) Lee, S.; Kim, S.; Choo, J.; Shin, S. Y.; Lee, Y. H.; Choi, H. Y.; Ha, S.; Kang, K.; Oh, C. H. Biological Imaging of HEK293 Cells Expressing PLCγ1 Using Surface-Enhanced Raman Microscopy. *Anal. Chem.* **2007**, *79*, 916–922.
(37) Faulds, K.; Barbagallo, R. P.; Keer, J. T.; Smith, W. E.; Graham, D. SERRS as a More Sensitive Technique for the Detection of Labelled Oligonucleotides Compared to Fluorescence. *Analyst* **2004**, *129*, 567–568.
(38) Wang, Y.; Yan, B.; Chen, L. SERS Tags: Novel Optical Nanoprobes for Bioanalysis. *Chem. Rev.* **2013**, *113*, 1391–1428.
(39) Kumar, P. S.; Pastoriza-Santos, I.; Rodríguez-González, B.; Abajo, F. J. G. de; Liz-Marzán, L. M. High-Yield Synthesis and Optical Response of Gold Nanostars. *Nanotechnology* **2008**, *19*, 15606.
(40) Rodríguez-Lorenzo, L.; Álvarez-Puebla, R. A.; Pastoriza-Santos, I.; Mazzucco, S.; Stéphan, O.; Kociak, M.; Liz-Marzán, L. M.; García de Abajo, F. J. Zeptomol Detection Through Controlled Ultrasensitive Surface-Enhanced Raman Scattering. *J. Am. Chem. Soc.* **2009**, *131*, 4616–4618.
(41) Esenturk, E. N.; High Walker, A. R. Surface-Enhanced Raman Scattering Spectroscopy via Gold Nanostars. *J. Raman Spectrosc.* **2009**, *40*, 86–91.
(42) Abramczyk, H.; Brozek-Pluska, B. Raman Imaging in Biochemical and Biomedical Applications. Diagnosis and Treatment of Breast Cancer. *Chem. Rev.* **2013**, *113*, 5766–5781.
(43) Su, X.; Zhang, J.; Sun, L.; Koo, T.-W.; Chan, S.; Sundararajan, N.; Yamakawa, M.; Berlin, A. A. Composite Organic−Inorganic Nanoparticles (COINs) with Chemically Encoded Optical Signatures. *Nano Lett.* **2005**, *5*, 49–54.
(44) Sun, L.; Sung, K.-B.; Dentinger, C.; Lutz, B.; Nguyen, L.; Zhang, J.; Qin, H.; Yamakawa, M.; Cao, M.; Lu, Y.; *et al.* Composite Organic−Inorganic Nanoparticles as Raman Labels for Tissue Analysis. *Nano Lett.* **2007**, *7*, 351–356.
(45) McCabe, A. F.; Eliasson, C.; Prasath, R. A.; Hernandez-Santana, A.; Stevenson, L.; Apple, I.; Cormack, P. A. G.; Graham, D.; Smith, W. E.; Corish, P.; *et al.* SERRS Labelled Beads for Multiplex Detection. *Faraday Discuss.* **2006**, *132*, 303–308.
(46) Samanta, A.; Maiti, K. K.; Soh, K.-S.; Liao, X.; Vendrell, M.; Dinish, U. S.; Yun, S.-W.; Bhuvaneswari, R.; Kim, H.; Rautela, S.; *et al.* Ultrasensitive Near-Infrared Raman Reporters for SERS-Based In Vivo Cancer Detection. *Angew. Chem. Int. Ed.* **2011**, *50*, 6089–6092.
(47) Yuan, H.; Liu, Y.; Fales, A. M.; Li, Y. L.; Liu, J.; Vo-Dinh, T. Quantitative SERRS Multiplexing of Biocompatible Gold Nanostars for in Vitro and Ex Vivo Detection. *Anal. Chem.* **2013**, *85*, 208–212.
(48) Driskell, J. D.; Kwarta, K. M.; Lipert, R. J.; Porter, M. D.; Neill, J. D.; Ridpath, J. F. Low-Level Detection of Viral Pathogens by a Surface-Enhanced Raman Scattering Based Immunoassay. *Anal. Chem.* **2005**, *77*, 6147–6154.
(49) Tam, N. C. M.; Scott, B. M. T.; Voicu, D.; Wilson, B. C.; Zheng, G. Facile Synthesis of Raman Active Phospholipid Gold Nanoparticles. *Bioconjug. Chem.* **2010**, *21*, 2178–2182.
(50) Ip, S.; MacLaughlin, C. M.; Gunari, N.; Walker, G. C. Phospholipid Membrane Encapsulation of Nanoparticles for Surface-Enhanced Raman Scattering. *Langmuir ACS J. Surf. Colloids* **2011**, *27*, 7024–7033.
(51) Tam, N. C. M.; McVeigh, P. Z.; MacDonald, T. D.; Farhadi, A.; Wilson, B. C.; Zheng, G. Porphyrin–Lipid Stabilized Gold Nanoparticles for Surface Enhanced Raman Scattering Based Imaging. *Bioconjug. Chem.* **2012**, *23*, 1726–1730.

(52) Mulvaney, S. P.; Musick, M. D.; Keating, C. D.; Natan, M. J. Glass-Coated, Analyte-Tagged Nanoparticles: A New Tagging System Based on Detection with Surface-Enhanced Raman Scattering. *Langmuir* **2003**, *19*, 4784–4790.
(53) Fernández-López, C.; Mateo-Mateo, C.; Álvarez-Puebla, R. A.; Pérez-Juste, J.; Pastoriza-Santos, I.; Liz-Marzán, L. M. Highly Controlled Silica Coating of PEG-Capped Metal Nanoparticles and Preparation of SERS-Encoded Particles. *Langmuir* **2009**, *25*, 13894–13899.
(54) Rodríguez-Lorenzo, L.; Krpetic, Z.; Barbosa, S.; Alvarez-Puebla, R. A.; Liz-Marzán, L. M.; Prior, I. A.; Brust, M. Intracellular Mapping with SERS-Encoded Gold Nanostars. *Integr. Biol.* **2011**, *3*, 922–926.
(55) Rodríguez-Fernández, D.; Langer, J.; Henriksen-Lacey, M.; Liz-Marzán, L. M. Hybrid Au–SiO2 Core–Satellite Colloids as Switchable SERS Tags. *Chem. Mater.* **2015**, *27*, 2540–2545.
(56) Mir-Simon, B.; Reche-Perez, I.; Guerrini, L.; Pazos-Perez, N.; Alvarez-Puebla, R. A. Universal One-Pot and Scalable Synthesis of SERS Encoded Nanoparticles. *Chem. Mater.* **2015**, *27*, 950–958.
(57) Freeman, R. G.; Doering, W. E.; Walton, I. D.; Penn, S. G.; Davis, G.; Wong, F.; Natan, M. J. Detection of Biomolecules Using Nanoparticle Surface Enhanced Raman Scattering Tags. In; 2005; Vol. 5705, pp. 114–122.
(58) Stokes, R. J.; Hernandez-Santana, A.; Macaskill, A.; Cormack, P. a. G.; Smith, W. E.; Graham, D. SERRS-Active Nanoparticle-Polymer Beads for Ultra-Sensitive Biodiagnostic Applications. *Micro Ampamp Nano Lett.* **2006**, *1*, 57–61.
(59) McLintock, A.; Hunt, N.; Wark, A. W. Controlled Side-by-Side Assembly of Gold Nanorods and Dye Molecules into Polymer-Wrapped SERRS-Active Clusters. *Chem. Commun.* **2011**, *47*, 3757–3759.
(60) Bodelón, G.; Montes-García, V.; Fernández-López, C.; Pastoriza-Santos, I.; Pérez-Juste, J.; Liz-Marzán, L. M. Au@pNIPAM SERRS Tags for Multiplex Immunophenotyping Cellular Receptors and Imaging Tumor Cells. *Small* **2015**, *11*, 4149–4157.
(61) Song, J.; Zhou, J.; Duan, H. Self-Assembled Plasmonic Vesicles of SERS-Encoded Amphiphilic Gold Nanoparticles for Cancer Cell Targeting and Traceable Intracellular Drug Delivery. *J. Am. Chem. Soc.* **2012**, *134*, 13458–13469.
(62) Yang, M.; Chen, T.; Lau, W. S.; Wang, Y.; Tang, Q.; Yang, Y.; Chen, H. Development of Polymer-Encapsulated Metal Nanoparticles as Surface-Enhanced Raman Scattering Probes. *Small* **2009**, *5*, 198–202.
(63) Soliman, M. G.; Pelaz, B.; Parak, W. J.; del Pino, P. Phase Transfer and Polymer Coating Methods toward Improving the Stability of Metallic Nanoparticles for Biological Applications. *Chem. Mater.* **2015**, *27*, 990–997.
(64) Ott, A.; Yu, X.; Hartmann, R.; Rejman, J.; Schütz, A.; Ochs, M.; Parak, W. J.; Carregal-Romero, S. Light-Addressable and Degradable Silica Capsules for Delivery of Molecular Cargo to the Cytosol of Cells. *Chem. Mater.* **2015**, *27*, 1929–1942.
(65) Harmsen, S.; Huang, R.; Wall, M. A.; Karabeber, H.; Samii, J. M.; Spaliviero, M.; White, J. R.; Monette, S.; O'Connor, R.; Pitter, K. L.; *et al.* Surface-Enhanced Resonance Raman Scattering Nanostars for High-Precision Cancer Imaging. *Sci. Transl. Med.* **2015**, *7*, 271ra7.
(66) Chen, G.; Teng, Z.; Su, X.; Liu, Y.; Lu, G. Unique Biological Degradation Behavior of Stöber Mesoporous Silica Nanoparticles from Their Interiors to Their Exteriors. *J. Biomed. Nanotechnol.* **2015**, *11*, 722–729.

(67) Zhai, W.; He, C.; Wu, L.; Zhou, Y.; Chen, H.; Chang, J.; Zhang, H. Degradation of Hollow Mesoporous Silica Nanoparticles in Human Umbilical Vein Endothelial Cells. *J. Biomed. Mater. Res. B Appl. Biomater.* **2012**, *100B*, 1397–1403.
(68) Izak-Nau, E.; Voetz, M.; Eiden, S.; Duschl, A.; Puntes, V. F. Altered Characteristics of Silica Nanoparticles in Bovine and Human Serum: The Importance of Nanomaterial Characterization prior to Its Toxicological Evaluation. *Part. Fibre Toxicol.* **2013**, *10*, 56.
(69) Zhang, F.; Lees, E.; Amin, F.; Rivera Gil, P.; Yang, F.; Mulvaney, P.; Parak, W. J. Polymer-Coated Nanoparticles: A Universal Tool for Biolabelling Experiments. *Small* **2011**, *7*, 3113–3127.
(70) Serrano-Montes, A. B.; Jimenez de Aberasturi, D.; Langer, J.; Giner-Casares, J. J.; Scarabelli, L.; Herrero, A.; Liz-Marzán, L. M. A General Method for Solvent Exchange of Plasmonic Nanoparticles and Self-Assembly into SERS-Active Monolayers. *Langmuir* **2015**, *31*, 9205–9213.
(71) Cancer Facts & Figures 2016; American Cancer Society http://www.cancer.org/research/cancerfactsstatistics/cancerfactsfigures2016/ (accessed May 25, **2016**).
(72) Holliday, D. L.; Speirs, V. Choosing the Right Cell Line for Breast Cancer Research. *Breast Cancer Res.* **2011**, *13*, 215.
(73) Vega, M. M.; Bonifacio, A.; Lughi, V.; Marsi, S.; Carrato, S.; Sergo, V. Long-Term Stability of Surfactant-Free Gold Nanostars. *J. Nanoparticle Res.* **2014**, *16*, 1–6.
(74) Guerrero-Martínez, A.; Barbosa, S.; Pastoriza-Santos, I.; Liz-Marzán, L. M. Nanostars Shine Bright for You: Colloidal Synthesis, Properties and Applications of Branched Metallic Nanoparticles. *Curr. Opin. Colloid Interface Sci.* **2011**, *16*, 118–127.
(75) Pierre, M. C. S.; Haes, A. J. Purification Implications on SERS Activity of Silica Coated Gold Nanospheres. *Anal. Chem.* **2012**, *84*, 7906–7911.
(76) Zhang, Y.; Walkenfort, B.; Yoon, J. H.; Schlücker, S.; Xie, W. Gold and Silver Nanoparticle Monomers Are Non-SERS-Active: A Negative Experimental Study with Silica-Encapsulated Raman-Reporter-Coated Metal Colloids. *Phys. Chem. Chem. Phys.* **2015**, *17*, 21120–21126.
(77) Hanwell, M. D.; Curtis, D. E.; Lonie, D. C.; Vandermeersch, T.; Zurek, E.; Hutchison, G. R. Avogadro: An Advanced Semantic Chemical Editor, Visualization, and Analysis Platform. *J. Cheminformatics* **2012**, *4*, 1–17.
(78) Nativo, P.; Prior, I. A.; Brust, M. Uptake and Intracellular Fate of Surface-Modified Gold Nanoparticles. *ACS Nano* **2008**, *2*, 1639–1644.
(79) Rivera-Gil, P.; Vazquez-Vazquez, C.; Giannini, V.; Callao, M. P.; Parak, W. J.; Correa-Duarte, M. A.; Alvarez-Puebla, R. A. Plasmonic Nanoprobes for Real-Time Optical Monitoring of Nitric Oxide inside Living Cells. *Angew. Chem. Int. Ed.* **2013**, *52*, 13694–13698.
(80) Yuan, H.; Khoury, C. G.; Hwang, H.; Wilson, C. M.; Grant, G. A.; Vo-Dinh, T. Gold Nanostars: Surfactant-Free Synthesis, 3D Modelling, and Two-Photon Photoluminescence Imaging. *Nanotechnology* **2012**, *23*, 75102.
(81) Pellegrino, T.; Manna, L.; Kudera, S.; Liedl, T.; Koktysh, D.; Rogach, A. L.; Keller, S.; Rädler, J.; Natile, G.; Parak, W. J. Hydrophobic Nanocrystals Coated with an Amphiphilic Polymer Shell: A General Route to Water Soluble Nanocrystals. *Nano Lett.* **2004**, *4*, 703–707.
(82) Lin, C.-A. J.; Sperling, R. A.; Li, J. K.; Yang, T.-Y.; Li, P.-Y.; Zanella, M.; Chang, W. H.; Parak, W. J. Design of an Amphiphilic Polymer for Nanoparticle Coating and Functionalization. *Small* **2008**, *4*, 334–341.

(83) Scarabelli, L.; Sánchez-Iglesias, A.; Pérez-Juste, J.; Liz-Marzán, L. M. A "Tips and Tricks" Practical Guide to the Synthesis of Gold Nanorods. *J. Phys. Chem. Lett.* **2015**, *6*, 4270–4279.

Table of Contents Graphic